

Design of a Dynamic Calibration Phantom to be used to calculate the Temporal Resolution of a Tomographic Imaging Device

by

Alexander Henry Slocum, Jr.

SUBMITTED TO THE DEPARTMENT OF MECHANICAL ENGINEERING IN PARTIAL FULFILLMENT OF THE REQUIREMENTS FOR THE DEGREE OF

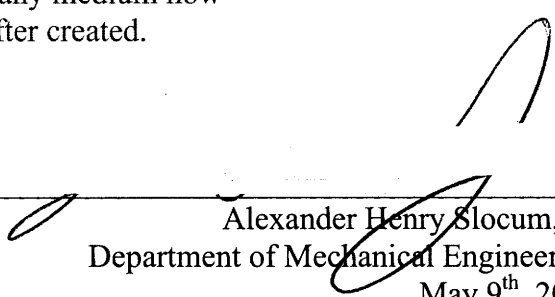
BACHELOR OF SCIENCE IN MECHANICAL ENGINEERING
AT THE
MASSACHUSETTS INSTITUTE OF TECHNOLOGY

June 2008

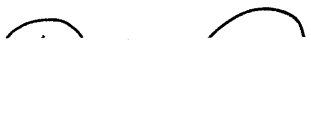
©2008 Alexander Henry Slocum, Jr. All rights reserved

The author hereby grants to MIT permission to reproduce and to distribute publicly paper and electronic copies of this thesis document in whole or in part in any medium now known or hereafter created.

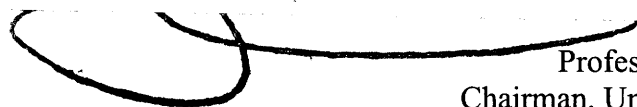
Signature of Author: _____

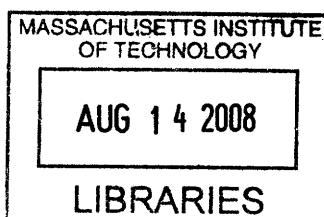

Alexander Henry Slocum, Jr.
Department of Mechanical Engineering
May 9th, 2008

Certified by: _____


Derek Rowell
Professor of Mechanical Engineering
Thesis Supervisor

Accepted by: _____


John H. Lienhard V
Professor of Mechanical Engineering
Chairman, Undergraduate Thesis Committee



ARCHIVES

Design of a Dynamic Calibration Phantom to be used to calculate the Temporal Resolution of a Tomographic Imaging Device

by

Alexander Henry Slocum, Jr.

Submitted to the department of Mechanical Engineering
on May 9th, 2008 in partial fulfillment of the
requirements for the degree of Bachelor of Science in
Mechanical Engineering

ABSTRACT

What follows is an account of the design and development of a calibration device for determining the temporal resolution of a tomographic imaging device. Current practice for characterizing the dynamic response of a tomographic imaging device, such as a Computed Tomography (CT) or Magnetic Resonance Imaging (MRI) machine, uses image acquisition time as a surrogate for temporal resolution.

At present, no standard method for characterizing the temporal resolution of a tomographic imaging device exists. Analogous to the spatial modulation transfer function used for characterizing spatial resolution, the concept of temporal Modulation Transfer Function (t-MTF) can be used to enable characterization of temporal resolution. A scanner's t-MTF represents the percent amplitude modulation in the image as a function of the input frequency.

The calibration device uses slotted disks mounted to planetary gear sets' rotating ring gears. The sun gears are driven by a common shaft, thus allowing for about two decades of input frequencies to be obtained using a single motor and driveshaft. Preliminary results show a monotonic decline in the temporal modulation transfer as the input signal frequency is increased. As was hypothesized, there is more modulation at lower frequency and less modulation at higher frequency. Analogous to the definition of spatial resolution, one can define the frequency for which there is 10% temporal modulation transfer as the temporal resolution of a scanner.

Thesis Supervisor: Derek Rowell
Title: Professor of Mechanical Engineering

Acknowledgments

The author would like to thank Dr. Rajiv Gupta for his excellent supervision and guidance for the duration of this project. In addition, Dr. Stephen Jones helped with design reviews for the temporal resolution phantoms, and was invaluable when it came to analyzing the output data from the CT scanners. The author would also like to thank his thesis advisor, Prof. Derek Rowell, for his supervision and guidance. Prof. Rowell's advice helped me develop a physical sense for large portions of the project that I had not thought of before, including the phantom design and the data analysis.

Prof. Alexander Slocum acted as a technical and editorial consultant during the course of this project. This work was supported in part by the Precision Engineering Research Group at MIT. Sophia Cheng at CIMIT was very helpful and assisted with ordering parts. Janet Galipeau, Joe Martino, and Paul McGrath at Maxon Motor Corporation were a pleasure to work with; they helped with selection of a motor and control system for the prototype device. Linda Denzer, Judy LaBonte, and Greg Mostovoy at Vaupell Rapid Solutions were extremely helpful and professional in getting parts for the prototype manufactured quickly and accurately. In addition, the staff at Renbrandt, Inc. was very helpful in selecting the motor coupling.

Dr. Mannudeep Kalra was extremely helpful, operating both the GE Lightspeed 64 and Siemens Sensation 64 scanners, allowing the device to be used to measure the temporal resolution of both scanners. Dr. Sarabjeet Singh was also very helpful in the data collection process for the GE Lightspeed scanner.

Peter Morley and the staff at MIT's Central Machine shop manufactured the protective case and mounting plate for the third iteration TRP. Mark Belanger at the Edgerton Student shop operated the 3-D printer used to manufacture the second iteration universal phantom. This research was funded through CIMIT grant number DAMD17-02-2-0006, sponsored by the U.S. Army Medical Research Acquisition Activity.

LIST OF FIGURES

Figure 1: CT Machine scanning bore. The X and Y axes are shown, with the sweet spot at their intersection.....	8
Figure 2: Temporal Resolution Phantom (Iteration 1).....	10
Figure 3: Cross-section of single planetary gear assembly.....	12
Figure 4: Front and rear views of a single gear assembly of the CT Calibration Tool iteration 2.	13
Figure 5: Overall view of assembly cross-section.	13
Figure 6: Close-up view of assembly cross-section.....	14
Figure 7: Bevel gears used to transmit torque from the motor shaft, which must be outside the scanning area, to the planetary gear sets' common driveshaft.....	15
Figure 8: Overall view of the second iteration.....	15
Figure 9: Third iteration Temporal Resolution Phantom.....	16
Figure 10: Close-up view of helical right-angle gearbox. Squeeze clamps are placed at shaft (3) and the opposite end of shaft (4).	17
Figure 11: Third iteration TRP in the bore of a CT scanner.....	18
Figure 12: Drive system and microcontroller being tested using the second iteration prototype	20
Figure 13: Detail of motor mounting and coupling.	20
Figure 14: Spatial resolution is calculated using the concept of line-pairs per centimeter. This is shown in the figure above.	21
Figure 15: Plot of spatial MTF, showing a monotonic decline in	21
Figure 16: Visual representation of the “actual modulation” of the input signal to the tomographic imaging device.....	22
Figure 17: Illustration of the “perceived” modulation output of the CT scanner.	23
Figure 18: The frequency simulation disk driven by the 34 tooth sun gear.	26
Figure 19: The frequency simulation disk driven by the 16 tooth sun gear.	26
Figure 20: Cross-section image of the Iteration II TRP generated using a clinical scanner.	28
Figure 21: The first iteration universal phantom disk.....	29
Figure 22: The second iteration universal phantom disk. Notice the increase in the event pair size.	31
Figure 23: Second iteration universal phantom, 3-D printed at the Edgerton Student Shop at MIT.	31
Figure 24: Modulation data. Each frequency produced by the TRP was registered by the Sensation-64 scanner and was assigned a grayscale value (measured in HU).	32
Figure 25: The t-MTF graph for the Sensation 64 scanner. Gantry was operated at a speed of one rotation per second. The temporal resolution, defined as the frequency at which there is 10% modulation transfer, is approximately 0.8 Hz.....	33
Figure 26: Plot of the temporal Modulation Transfer Function for two different CT scanners.....	34
Figure 27: The temporal resolution is the frequency at which each scanner achieves 10% modulation transfer. For the GE, this is 1.6Hz, and for the Siemens, this is 1.84 Hz.	34

LIST OF TABLES

Table 1: Functional Requirements for a Temporal Resolution Phantom.	9
Table 2: Motor and Gear Parameters	10
Table 3: Planetary Gear Drive Analysis	11
Table 4: Weight Supported by Bearings.....	18
Table 5: Calculation of Drag Torque from Bearings.....	18
Table 6: Calculation of System Acceleration Torque.....	19
Table 7: Calculating internal gear frequency.....	24
Table 8: Calculating number of EPs	24
Table 9: Frequency error analysis.....	25
Table 10: EPs calculations	25
Table 11: Calculation of Event Pair arc length for driveshaft speeds of 20 and 40 RPM.	27
Table 12: TRP Disk Iteration 2 Frequency Analysis	29
Table 13: Calculating required number of event pairs.....	30
Table 14: Determination of event pair size.....	30

TABLE OF CONTENTS

- 1 Introduction** 7
- 2 Methods**..... 8
 - 2.1 *Functional Requirements* 8
 - 2.2 *Design Iteration I*..... 9
 - 2.3 *Design Iteration II*..... 11
 - 2.4 *Design Iteration III* 15
 - 2.5 *Determination of Appropriate Motor Size* 18
 - 2.6 *Temporal Modulation Transfer Function (t-MTF)* 20
 - 2.7 *Phantom Disk Design – Iteration I*..... 23
 - 2.8 *Phantom Disk Design - Iteration II (Universal Phantom)*..... 28
 - 2.9 *Universal Phantom Iteration II*..... 30
- 3. Results and Discussion**..... 31
 - 3.1 *Iteration II (Proof-of-Concept)* 31
 - 3.2 *Iteration III*..... 33
- 4. Conclusions** 35
- References**..... 36

Design of a Dynamic Calibration Phantom to be used to calculate the Temporal Resolution of a Tomographic Imaging Device

1 Introduction

Tomographic imaging devices, such as computed tomography (CT) and magnetic resonance imaging (MRI) machines are increasingly used for visualizing dynamic processes, such as a beating heart and the perfusion of organs [1]. In addition, they can now render high contrast and spatial resolution (up to 150 microns in-plane for certain scanners). The increasingly powerful capabilities of CT and MRI scanners have stimulated research in the development of high-quality imaging in real-time (4-D imaging), also known as dynamic imaging. Dynamic imaging is now also increasingly used to create images of time-varying processes that previously were obtained using standard MRI or CT technology [2].

One type of scanner that holds great promise in dynamic imaging is the flat-panel Volumetric Computed Tomography (fp-VCT). Introduced in the 1990s, fp-VCT is a significant advance from the “conventional” CT scanner, and it represents a unique design capable of ultra-high spatial resolution as well as dynamic CT scanning [2]. Combined with its special flat-panel design, fp-VCT utilizes mathematical algorithms to create accurate 4-D representations of the human body, which can aid physicians in the detection and diagnosis of disease. These 4-D images also have the potential to be used in the development of new treatments and interventional procedures.

Despite its potential, dynamic imaging is relatively new and there are technical issues that need to be resolved before it can be used accurately and reliably for broad clinical applications. One significant issue is that objective measurement of a scanner’s temporal resolution is currently not possible. In contrast to spatial resolution, which can be easily calibrated using existing static phantoms, the measurement of temporal resolution remains elusive. While a method for defining and measuring spatial resolution in terms of modulation transfer function exists, there is no standard method for measuring temporal resolution.

A new device and method for measuring and characterizing temporal resolution has been developed as the subject of this thesis, using a modulation transfer function similar to that currently used to characterize spatial resolution. The method is referred to as the *Temporal Modulation Transfer Function*, or t-MTF. For a time-varying signal, t-MTF describes how well signal amplitude modulation in the object space is represented in the image space. It is believed that there is a direct correlation between image modulation and the signal frequency, similar to the dependence of optical image quality on spatial frequency seen in optical systems [3].

The new device is a dynamic calibration phantom which uses rotating slotted disks to generate square wave signals of different frequencies. These disks are mounted on a series of planetary gear sets’ rotating ring gears, whose sun gears are driven by a common shaft and whose planet support shafts are fixed. Through this arrangement, up to two decades or more of scan-able input frequencies can be generated using a single motor and driveshaft. Multiple iterations of the device were conceived during the project. In the final iteration, four of these planetary gear assemblies have been placed inside of a clear, protective cylindrical housing, in the manner of currently available static phantoms.

2 Methods

The design of the device, known as a *Temporal Resolution Phantom* (TRP), began with the idea of using a series of planetary gear assemblies driven by a common shaft to achieve a wide range of rotational velocities, each to be used to generate spatial signals (to be sensed by a tomographic scanner) with pre-determined frequencies in order to measure a scanner's temporal resolution. A series of multiple planetary gear assemblies spaced closely together enables the use of many similar parts and the ability to power many stages with a common driveshaft.

The image quality of the scanner varies with respect to the object's position inside the scanning volume. The isocenter, or "sweet spot", is located at the intersection of the X and Y-axes as seen in Figure 1, which also shows the second iteration proof-of-concept TRP. The isocenter is the most sensitive part of the machine and provides the highest scanning resolution. The optimal placement of the TRP is thus when it is located as close to the isocenter of the imaging device as possible. A list of functional requirements for the device was first generated, and the functional requirement of spacing multiple rotating calibration disks close together in order to get them as close to the isocenter as possible stems from this characteristic of the imaging device.

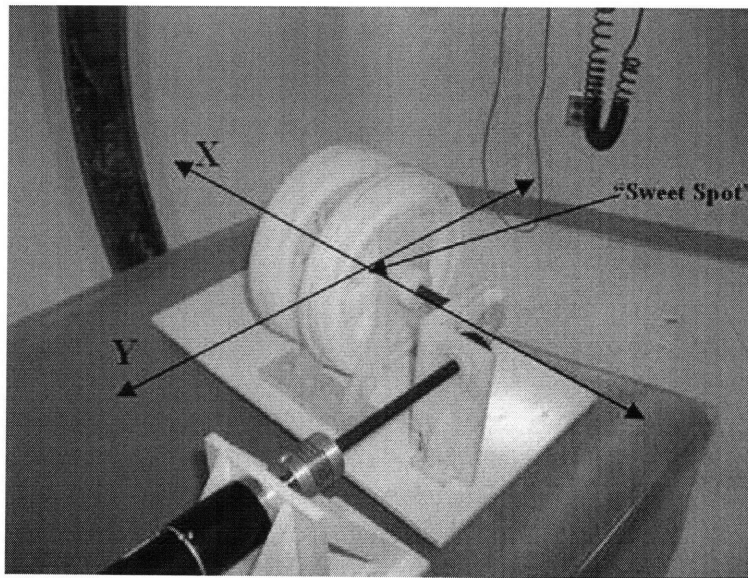


Figure 1: CT Machine scanning bore. The X and Y axes are shown, with the sweet spot at their intersection.

2.1 Functional Requirements

The first step in the design process was to determine a set of functional requirements that would adequately describe the device's intended functionality. Table 1 shows a list of these functional requirements. Possible design parameters are listed as well in order to foreshadow certain designs that were used in the final prototype.

Table 1: Functional Requirements for a Temporal Resolution Phantom.	
Functional Requirements	Design Parameters
Low X-ray attenuation characteristics	Appropriate materials limited by a scanner's sensitivity to metals and similarly dense objects. Plastics were the primary material used in the fabrication of the device.
Simulate a large range of input frequencies (speeds)	Method of simulating frequencies must be visible to tomographic imaging devices.
Accurate differential speed	Planetary gear assemblies. Multiple assemblies can be driven by one shaft. Internal gear must be a common part among all assemblies to minimize cost.
Small volume and profile	Fits into scanning volume of imaging device; satisfied by planetary gear assemblies.
Easy to operate	Requires almost no setup. Easy to operate, to limit human error.

In addition to the volume limitations placed on the device, the need for very precise velocity control is evident due to the fact that small variations in the velocity of the internal gear assemblies during data collection could cause variations in the output of the imaging device. Conventional spur gears, which are good at precision velocity transmission, are low cost and would enable the device to be easily manufactured [4]. Successive generations of the device could utilize helical gears, and the axial forces generated would also act to help preload the plastic ball bearings¹ [5]. Since this device operates at relatively low constant speed with no external loads, the Module 1 teeth were chosen to enable ease of manufacturing by rapid prototyping [5].

2.2 Design Iteration I

The first iteration of the TRP was based on a common planetary gear train with a sun gear driving a fixed planet gear, which moves the outer internal ring gear assembly. As seen in Figure 2, iteration 1 featured a large bearing with an internal gear cut into an extended inner raceway. There are 5 main components:

1. *Bearing outer raceway* for internal ring gear cut into outer disk.
2. *Sun gear* mounted on driveshaft (not pictured).
3. *Planet gear* mounted on fixed shaft on inner fixed planet carrier and driven by sun gear;
4. *Inner raceway* for internal gear bearing cut onto OD of inner fixed planet carrier.
5. *Internal gear* cut into outer disk, driven by planet gear

¹ www.kmsbearings.com.

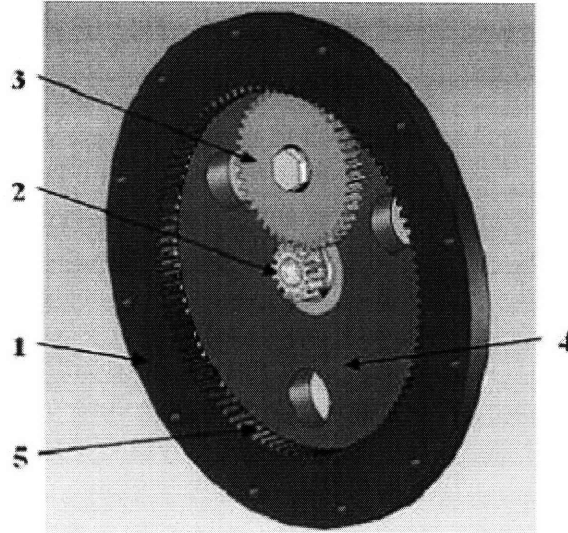


Figure 2: Temporal Resolution Phantom (Iteration 1).

A large range of speeds was initially desired because this would allow the scanner to image multiple elements simultaneously. A typical data collection event was estimated to take about 30 seconds. If ten inputs were required, then scanning one single assembly for each desired input would take ten times as long as using ten staggered assemblies. Furthermore, this simple estimate does not take into account the time associated with switching out each of ten assemblies.

To reduce cost and eliminate part count, all internal ring gears were to be the same. This was achieved by setting the pitch diameter of the internal gear to a constant value *const*, and using the following criteria:

1. Maintain a constant pitch radius in the internal gear, as well as the planet and sun gear diameters that are solutions to Equation (1):

$$const = \frac{D_{pitch-internal}}{2} = D_{pitch-planet} + \frac{D_{pitch-sun}}{2} \quad \text{Eq. (1)}$$

2. Utilizing the design parameters specified by the radiologist, the reductions in gear ratios were calculated:

A 10% reduction in speed from each successive assembly to the next was initially outlined as the ideal configuration. However, the analysis will show that this is not possible. Table 2 shows drive motor and gear parameters, while Table 3 shows the bulk of the spreadsheet used in the analysis.

Shaft Speed	100	Rpm
Internal Gear Diameter	100	mm
Module	1	mm/tooth

Sun Gear				Planet Gear	
Diameter	Number of Teeth	Gear Ratio	Speed Ratio	Diameter (mm)	Number of Teeth
14.0	14.0	0.14		43.0	43.0
16.0	16.0	0.16	14.29%	42.0	42.0
18.0	18.0	0.18	12.50%	41.0	41.0
20.0	20.0	0.2	11.11%	40.0	40.0
22.0	22.0	0.22	10.00%	39.0	39.0
24.0	24.0	0.24	9.09%	38.0	38.0
26.0	26.0	0.26	8.33%	37.0	37.0
28.0	28.0	0.28	7.69%	36.0	36.0
30.0	30.0	0.3	7.14%	35.0	35.0
32.0	32.0	0.32	6.67%	34.0	34.0
34.0	34.0	0.34	6.25%	33.0	33.0
36.0	36.0	0.36	5.88%	32.0	32.0
38.0	38.0	0.38	5.56%	31.0	31.0
40.0	40.0	0.4	5.26%	30.0	30.0
42.0	42.0	0.42	5.00%	29.0	29.0

All gears used in this device are metric, with a Module of one. For this fixed planet carrier design, the gear ratio is the ratio of each respective sun gear pitch diameter to the constant pitch diameter of the internal gear. Speed ratio refers to the reduction in speed between successive planetary gear assemblies.

Concerning the initial desired 10% speed reduction between assemblies, the analysis shows that this is unobtainable. However, the results were still satisfactory. For the second iteration prototype, assemblies with sun gear diameters of 16 and 34 mm were manufactured as a proof-of-concept, seen as bold in Table 3.

One constraint that was considered while choosing gear ratios for the first prototype was the diameter of the driveshaft. It was determined that an 8 mm diameter shaft would enable a relatively small sun gear to be used while still providing enough stiffness to the system given the required spacing of the planet and internal gear supports.

Planetary gear assemblies were completed using two different sun gear sizes. The 16 tooth gear was chosen because it was the smallest gear with well-formed teeth that could be mounted on the 8 mm central common drive shaft. The second gear assembly, using the 34 tooth gear, was chosen primarily to achieve a respectable difference in speeds.

2.3 Design Iteration II

Through the use of the Peer Review Evaluation Process (PREP) [6], the design evolved to a free-standing configuration. The bearing that was integral with the internal gear was removed due to concerns over part cost.

The new design uses stock plastic ball bearings (KMS Bearing Part number A606-P)². In addition, it allows for a more robust setup, with each successive internal gear mounted on its own separate single-planet-gear drive train. The second iteration planetary gear assembly, shown in Figure 3, has 7 primary components:

1. *Sun gear* mounted to driveshaft via keyway (driveshaft and keyway not pictured).
2. *Planet gear* mounted on fixed shaft on inner fixed planet carrier, which also serves as support for the assembly; driven by sun gear.
3. *Internal gear* driven by the planet gear.
4. *Planet gear mounting shaft*.
5. Plastic Conrad-type bearings mounted back-to-back using spacers.
6. *Internal gear bearing preload cover*.
7. *System assembly support* which also functions as planet carrier.

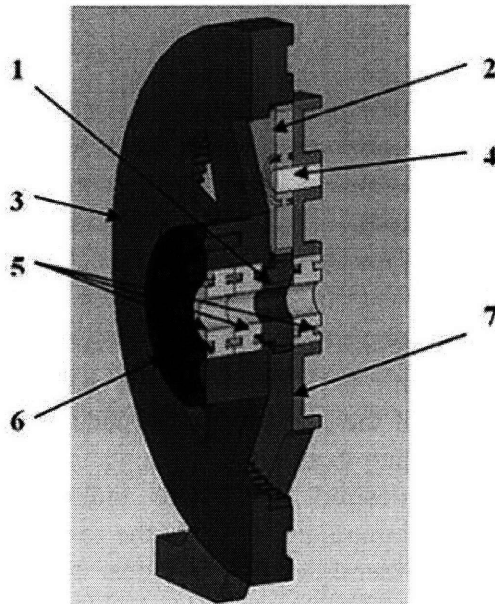


Figure 3: Cross-section of single planetary gear assembly.

Concentricity of the internal gear and the drive shaft is maintained by the plastic Conrad-type ball bearings. As a result, only one spur-tooth-based planet gear is needed for power transmission. Note that if helical gear teeth were used, which would have resulted in smoother velocity transmission, it would have been necessary to use two or three planets in order to prevent a moment from being placed on the ring gear [5]. A single plastic Conrad bearing is mounted on the planet gear support shaft to directly support the planet gear, such that the gear tooth forces pass directly through the bearing raceways.

Figure 4 shows front and rear views of the second iteration single stage assembly. Each system assembly support provides support to two internal gear assemblies, as can be seen in Figures 5 and 6.

²www.kmksbearings.com.

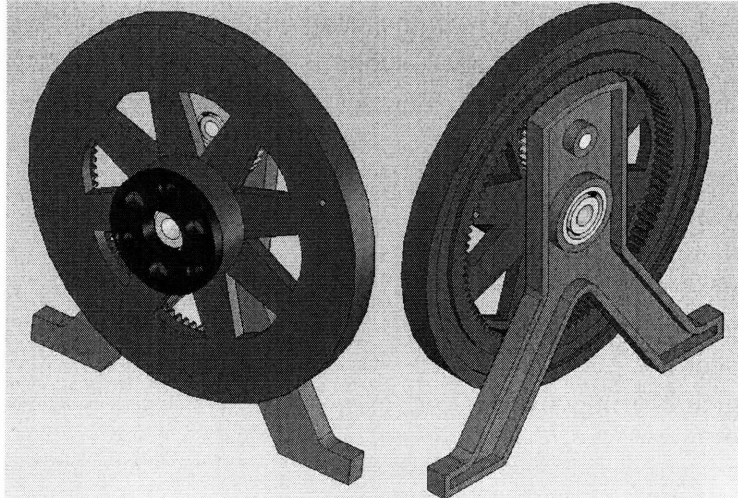


Figure 4: Front and rear views of a single gear assembly of the CT Calibration Tool iteration 2.

The internal gear supports provide support for the two closest internal gear assemblies, thus minimizing sine error misalignments (a variation of Abbe's principle). A shaft diameter of 8 mm can accommodate a bearing spacing of up to 80 mm (based on Saint Venant's principle) while controlling angular errors of mounted components [7]. Figure 5 shows a cross-section of the entire assembly. Note that the planet gear mounting shaft (component 4 in Figure 3) has been replaced by a shaft molded into the surface of the internal gear support.

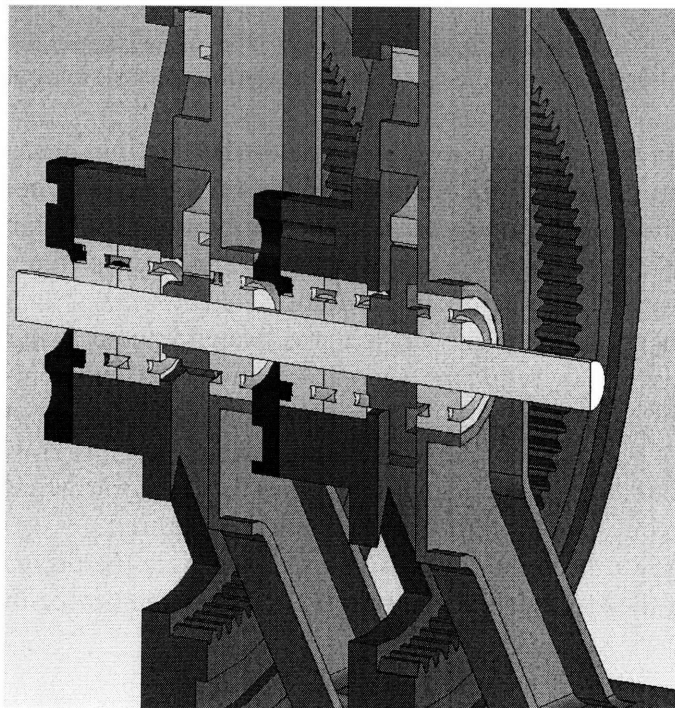


Figure 5: Overall view of assembly cross-section.

Figure 6 shows a close-up of the cross-section seen in Figure 5. The inner distance between the two internal gear supports is 30mm. The components shown in Figure 6 include:

1. Internal gear supports
2. Internal gear 1 bearings
3. Driveshaft support bearings
4. Driveshaft
5. Internal gear 1
6. Internal gear 2
7. Internal gear bearing cover

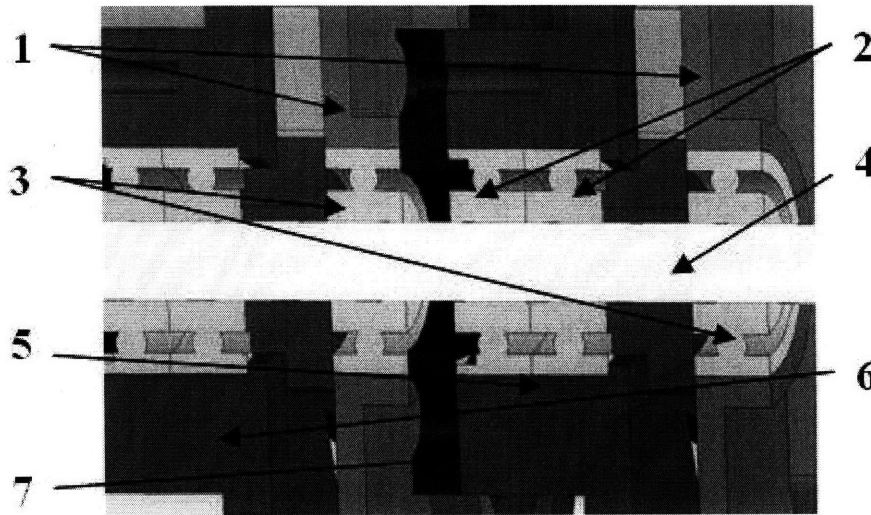


Figure 6: Close-up view of assembly cross-section.

As shown in Figure 6, the axial spacing of the bearings that support the internal ring gear is small in relation to the diameter of the ring gear. This could possibly lead to some tilt error motion of the ring gear and the calibration disk which is mounted to it. However, this is a non-sensitive direction with respect to the measurement of a tomographic imaging device's temporal resolution.

The second iteration of the device was manufactured using stereo-lithography (SLA) rapid-prototyping³. After the second iteration test with only two internal gear assemblies, the initial strategy of using multiple internal gear assemblies was re-evaluated. It did not seem feasible to use ten different assemblies as was initially planned. Instead, a multi-slotted disk which would attach to the ring gear was designed to simulate multiple speeds, so only two or three stages would be required.

Figure 7 shows the right angle drive used to enable the drive motor to be located outside the bore of the CT machine, and Figure 8 shows the device inside the bore of the CT machine.

³ www.vaupell.com.

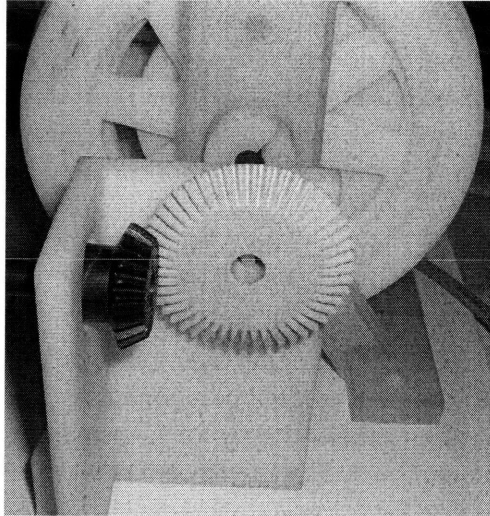


Figure 7: Bevel gears used to transmit torque from the motor shaft, which must be outside the scanning area, to the planetary gear sets' common driveshaft.

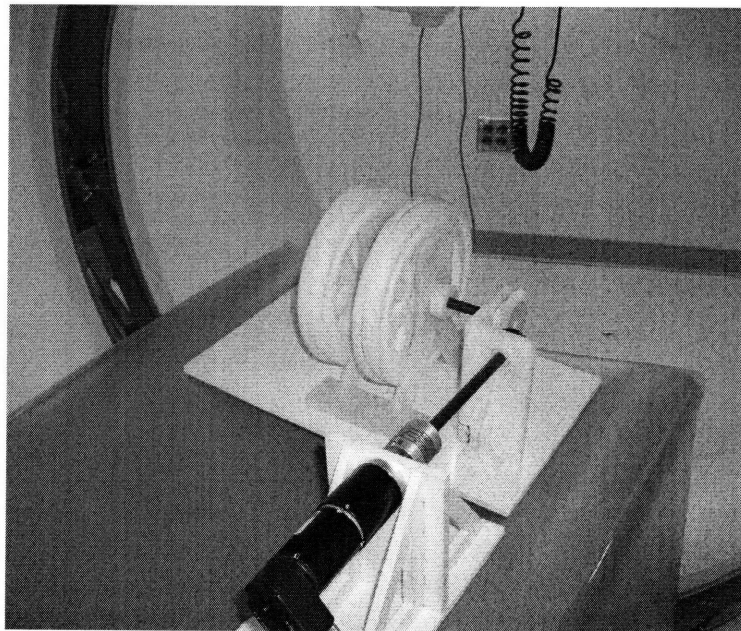


Figure 8: Overall view of the second iteration.

2.4 Design Iteration III

Preliminary tests showed that the proof-of-concept was capable of generating data showing a monotonic decline in the temporal resolution with increasing temporal frequency. The physicians then expressed their desire to design a testing platform that was capable of driving multiple different phantom designs, so that an optimal phantom disk design could be found. As such, the design of the device was adjusted slightly. One benefit of this design change would be that this new “platform” would help to minimize the cost of successive TRP iterations. It would only be necessary to change the design of the phantom disks.

For the third iteration, the number of planetary gear sets was increased from two to four. This was done primarily to allow for greater flexibility of the system, and to accommodate additional phantoms if necessary. The third iteration TRP, shown in Figure 9, has the same basic components as the second iteration. However, some elements of the design have been changed, as highlighted by the following points:

1. *Acrylic Tube* isolates and protects the phantoms.
2. *Two additional planetary gear drives* which allow for an increased range of input frequency signals.
3. *Acrylic Mounting Plate* allows for easy removal and access to the TRP for servicing and/or replacement of TRP components outside of the tube.
4. *Right angle gearbox* that allows the motor to transmit torque to the planetary gear driveshaft from outside the scanner field of view.

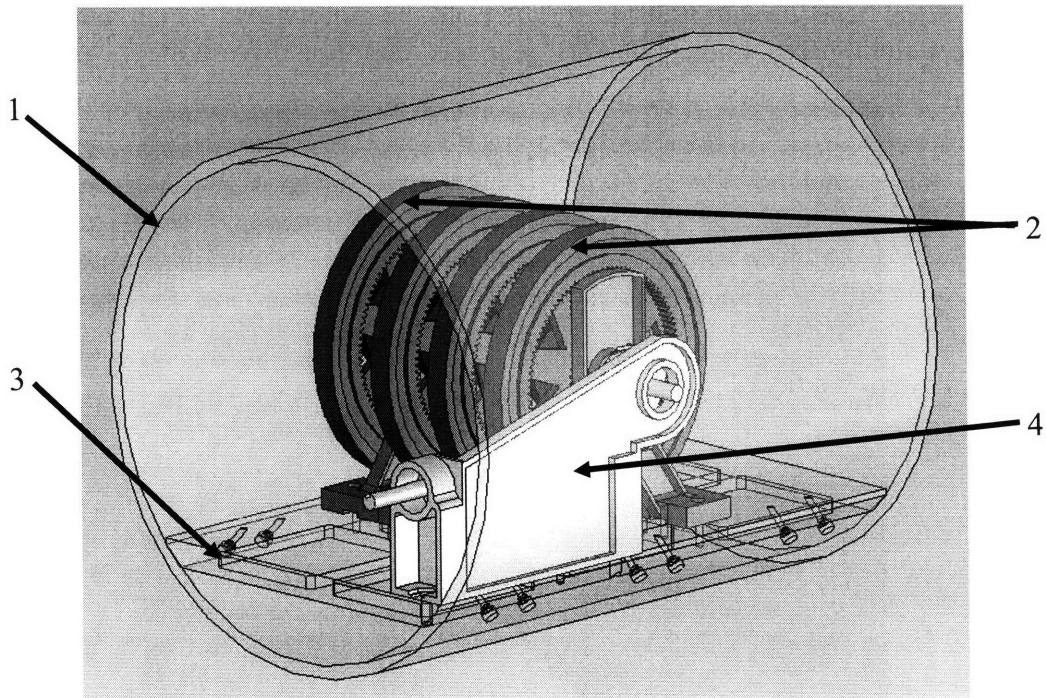


Figure 9: Third iteration Temporal Resolution Phantom

What cannot be seen adequately in Figure 9 is that the right-angle gearbox now uses a helical gear set to transmit the torque from the motor output shaft to the planetary gear drive shaft. The helical gears generate axial forces on both shafts, and these forces are resisted via utilization of squeeze clamps, placed on both shaft ends visible in Figure 9. The direction of rotation of the phantom is such that these are the only two locations that require placement of squeeze clamps to resist axial forces. Additionally, the phantom is only rotated in a single direction during a scan, so each shaft only requires one squeeze clamp.

No squeeze clamps are shown in these figures, but they were placed on the shafts before the device was used. Figure 10 shows several additional features not depicted in Figure 9. They are labeled as follows:

1. *Right angle gearbox* allows transmission of torque from the motor output shaft to the planetary gear drive shaft.
2. *Helical gear set* used to transmit torque from the motor output shaft to the planetary gear sets.
3. *Planetary gear shaft* used to drive the planetary gear sets.
4. *Motor output shaft* that drives the system from outside of the scanner field of view.

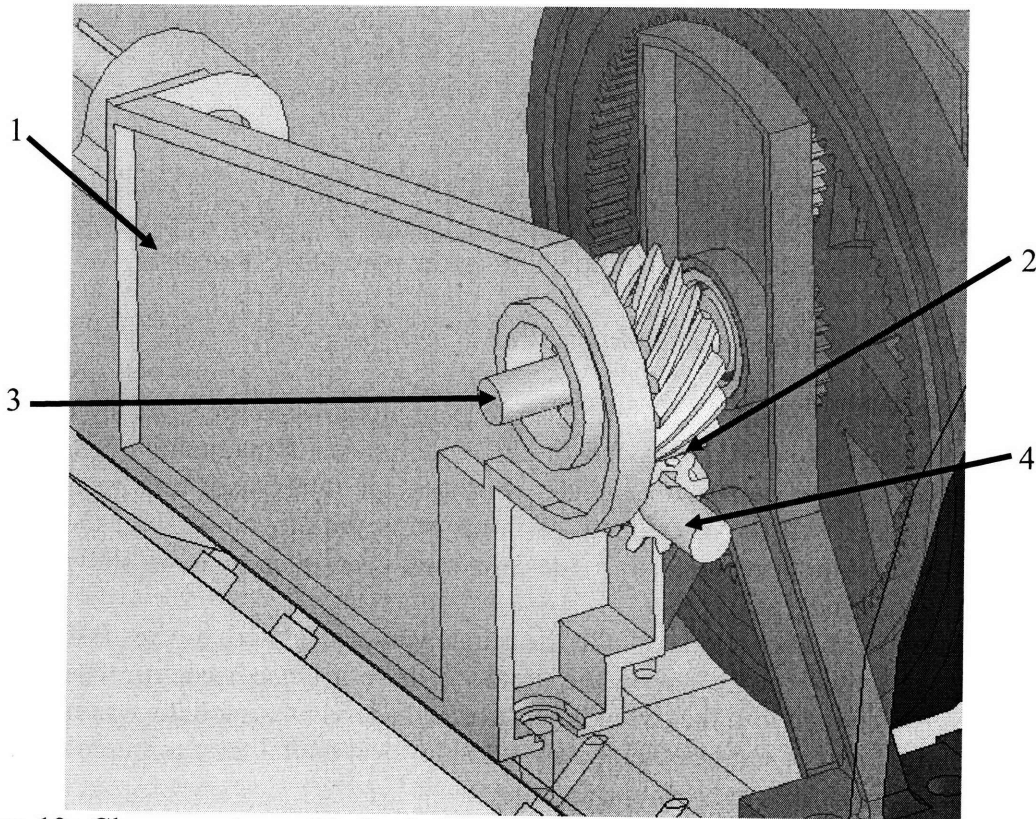


Figure 10: Close-up view of helical right-angle gearbox. Squeeze clamps are placed at shaft (3) and the opposite end of shaft (4).

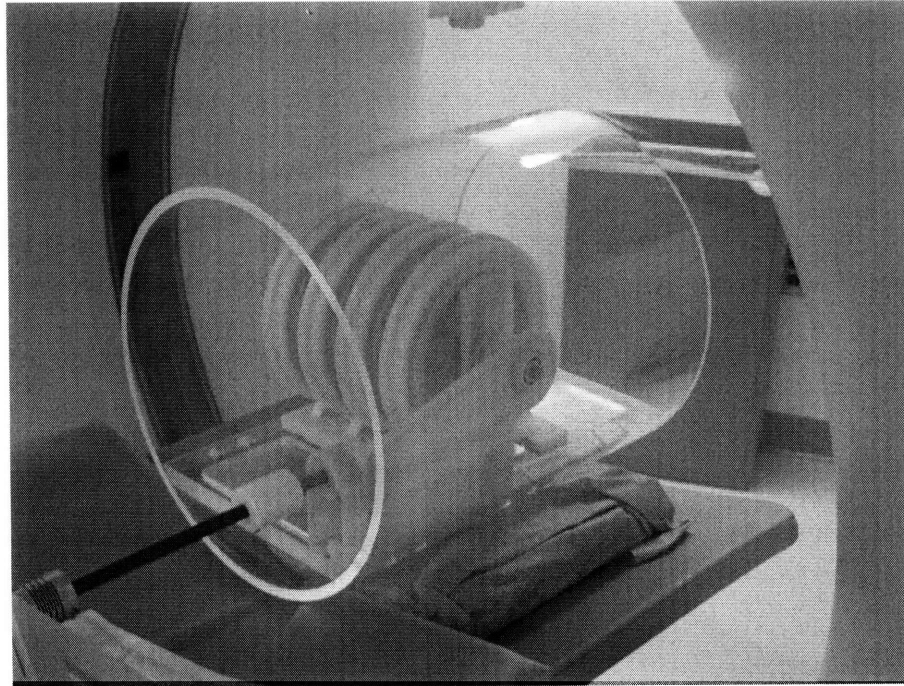


Figure 11: Third iteration TRP in the bore of a CT scanner.

2.5 Determination of Appropriate Motor Size

The initial prototype was powered using an unknown-source DC motor that was driven open loop. However, because of the importance of maintaining constant disk velocity, a precision motor (with encoder feedback for future use) was purchased. The motor was sized based on an estimate of initial static torque, along with the estimated maximum motor output required to rotate 2 internal gear assemblies, as shown in tables Table 4, Table 5, and Table 6.

The weight supported by the bearings was calculated to be 7.30 N for 4 assemblies, in anticipation of using the motor to drive a larger system. The light load friction coefficient between the nylon inner race and acetyl bearing balls was measured to be 0.18. Summation of torques yielded an estimate for the total drag torque of 0.0104 N-m.

Table 4: Weight Supported by Bearings		
Weight of planetary gear assembly	1.82	N
Number of assemblies	4	
Weight of Drive Shaft	0.102	N
Total weight supported by bearings	7.30	N

Table 5: Calculation of Drag Torque from Bearings		
Bearing friction coefficient	0.18	
Bearing ball drag force	1.31	N
Bearing ball pitch radius	0.0079	m
Bearing Drag Torque	0.0104	N-m

SolidWorks™ solid-models (similar to those shown in Figures Figure 3, Figure 4 and Figure 5) of the device were used to calculate the rotational moment of inertia of each component in the assembly, as seen in Table 6.

Table 6: Calculation of System Acceleration Torque		
Internal gear assembly inertia	0.0005	kg*m ²
Number of planetary gear assemblies	4	
Planetary gear assembly inertia	0.002	kg*m ²
Phantom disk inertia	0.0002	kg*m ²
Number of phantom disks	4	
Total phantom disk inertia	0.0008	kg*m ²
System Inertia	0.003	kg*m ²
Maximum Rotational Velocity	1.05	rad/sec.
Velocity rise time	0.5	sec.
Maximum acceleration	2.1	rad/sec. ²
Torque required for acceleration	0.006	N-m
Safety Factor	3	
Gear Friction Factor	6	
Desired motor output torque	0.29	N-m

A Maxon Motor model EC30 was selected, along with an integral HP optical encoder and 111:1 gearbox. Figure 12 is a view of the overall drive system showing the motor, encoder and gearbox, and the microcontroller. Figure 13 shows the coupling used to account for misalignment in the system,⁴ along with the gearbox and motor mount. Key features labeled in the following two figures are as follows:

1. *Maxon motor* used to supply torque to the temporal resolution phantom.
2. *Optical encoder* mounted on the motor used to provide closed-loop velocity control of the motor.
3. *Microcontroller* used to control the velocity and torque output of the motor.
4. *Helical beam coupling* attaches the motor output shaft to the input shaft of the phantom.
5. *Motor mount* used to stabilize the motor and provide constraint.

⁴ Renbrandt couplings (www.renbrandt.com).

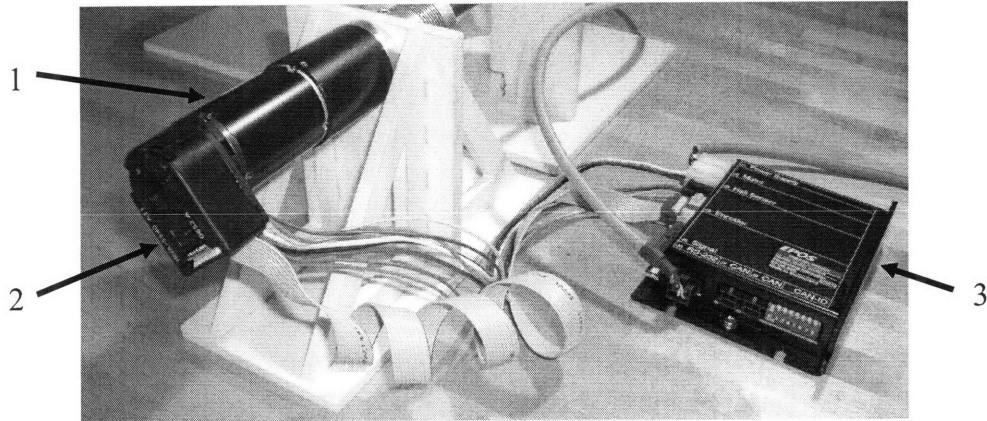


Figure 12: Drive system and microcontroller being tested using the second iteration prototype

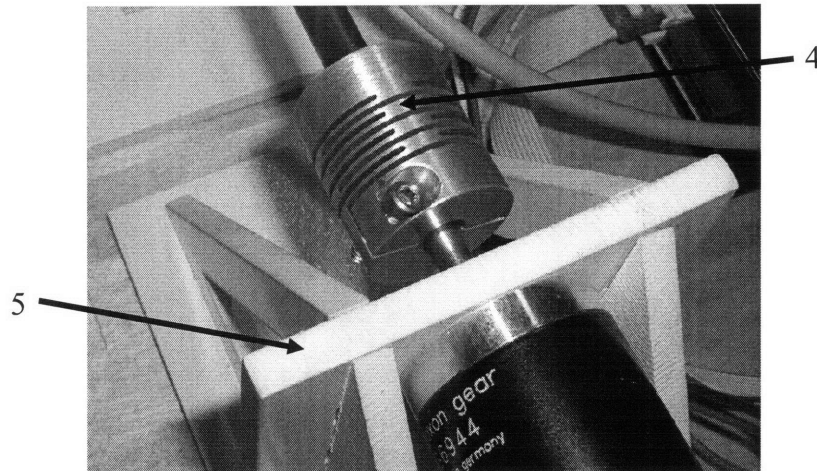


Figure 13: Detail of motor mounting and coupling.

2.6 Temporal Modulation Transfer Function (t-MTF)

Temporal Modulation Transfer Function is the time-analog of Spatial Modulation Transfer Function (spatial MTF). Figure 14 demonstrates the concept of spatial frequency, defined in units of line-pairs per centimeter (lp/cm). A line-pair consists of one light line and the adjacent dark line. As the number of line pairs per centimeter is increased, the ability to distinguish between successive light and dark lines decreases. Figure 14 shows a spread of spatial frequencies ranging from 16 lp/cm to 21 lp/cm.

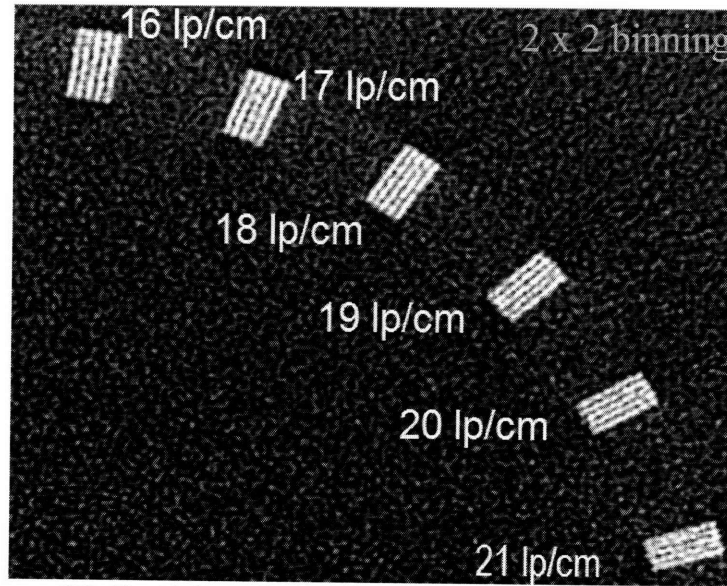


Figure 14: Spatial resolution is calculated using the concept of line-pairs per centimeter. This is shown in the figure above.⁵

Figure 15 shows a plot of spatial MTF, from which can be seen that the spatial modulation transfer decreases with increasing spatial frequency. Using the spatial MTF plot, the spatial resolution is defined as the spatial frequency for which there is 10% spatial modulation transfer. The spatial resolution of a tomographic imaging device is thus determined by its ability to resolve a spread of given spatial frequencies.

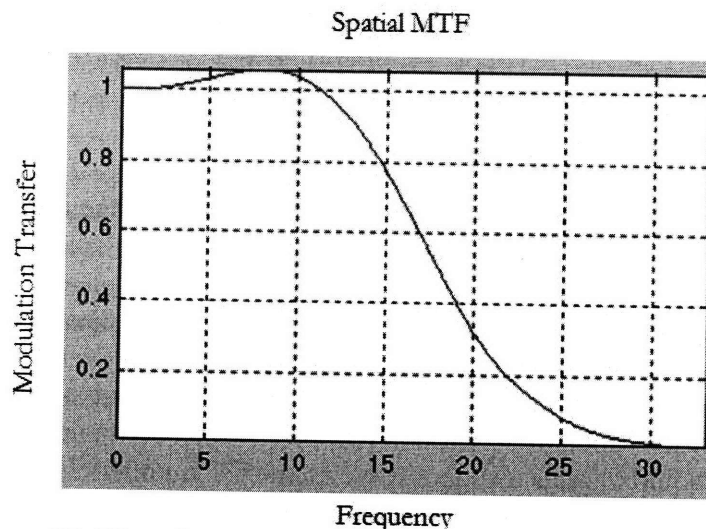


Figure 15: Plot of spatial MTF, showing a monotonic decline in Spatial Modulation Transfer with increasing spatial frequency.⁵

As stated previously, t-MTF is the time-analog of spatial MTF and is calculated given a measurement of the tomographic imaging device's ability to resolve increasing spatial frequencies. The purpose of the TRP is to generate signals which the tomographic

⁵ These figures courtesy of Dr. Rajiv Gupta, Department of Radiology, Massachusetts General Hospital

imaging device is capable of resolving, of increasing spatial frequency, so as to determine the temporal resolution of the imaging device. The concept of event-pairs (EPs) is now introduced. EPs are the time-analog of the spatial equivalent, line-pairs. An event pair consists of a section of plastic, and an equally sized adjacent section of air.

This embodiment of the TRP utilizes event pairs arranged in a circular pattern on a disk (as discussed in Sections 2.7 – 2.9), which is then rotated by planetary gear assemblies. The tomographic imaging device resolves the difference between plastic and air based on the differing CT numbers of air and plastic. Each circular arrangement of EPs creates a square wave of uniform “troughs” and “plateaus” of varying density in the object domain; this is the “actual modulation” of the input signal. This concept is illustrated by Figure 16.

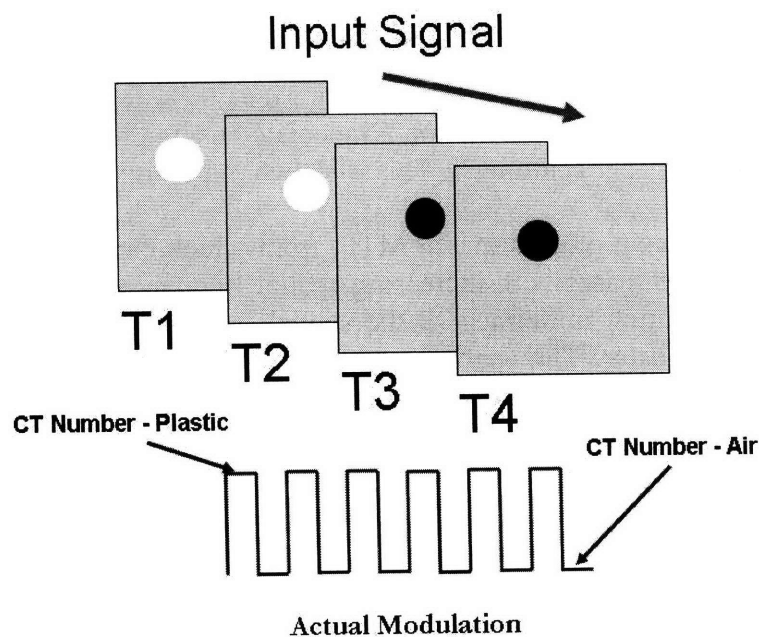
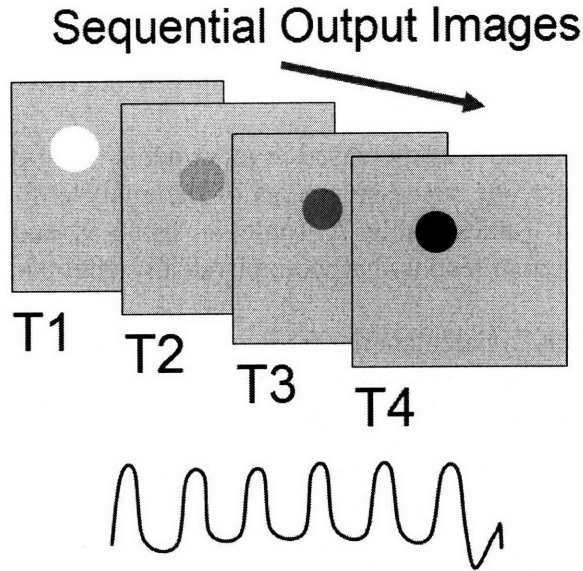


Figure 16: Visual representation of the “actual modulation” of the input signal to the tomographic imaging device (image courtesy Dr. Rajiv Gupta).

When the TRP is scanned with a tomographic imaging device, the plane of image acquisition is perpendicular to the plane of disk rotation. The event pairs rotate through the plane of image acquisition, generating the time-varying input signal. If one considers the CT number, or the Hounsfield Units (HUs), of a voxel through which the event pairs rotate, ideally it should vary as a square wave as the CT number changes from that of air, to that of plastic, and back again. From this aspect of the device the input, or “actual”, modulation is defined as the difference between the HUs of plastic and air.

In the imaging domain, consisting of the output of the tomographic imaging device, there will be blurring of event pair images because of the imaging devices limited ability to resolve the discontinuities in the square wave signal. This is the “perceived modulation” of the input signal, as demonstrated in Figure 17. The information about the temporal resolution resides in the degree to which blurring occurs for various input frequencies.



Perceived Modulation
Figure 17: Illustration of the “perceived” modulation output of the CT scanner (image courtesy Dr. Rajiv Gupta).

One can measure this variation in the image domain to compute the modulation transfer for each frequency, defined by Equation 2:

$$\text{Modulation Transfer} = \frac{\text{Max}_{HU} - \text{Min}_{HU}}{\text{Plastic}_{HU} - \text{Air}_{HU}} \quad \text{Eq. (2)}$$

The numerator represents the HU range measured by the imaging device for a given frequency. Conversely, the denominator represents the difference in the HUs of plastic and air (a range that should ideally be present if the scanner had infinitesimal temporal resolution). HU values are converted to grayscale values and the signal modulation is calculated, correlated with the respective frequency, and used to generate a plot of the scanner’s temporal Modulation Transfer Function (t-MTF). This plot can then be used to pinpoint the scanner’s temporal resolution.

2.7 Phantom Disk Design – Iteration I

In medical imaging, a phantom refers to an object that is used in some cases to represent anatomical features of biological organisms, and in others to allow operators to calibrate different characteristics of the imaging device. It was determined that inputs of different frequencies could be simulated through the use of slotted plastic disks. These were to be mounted to the internal gears, in order to provide a surface on which to project a desired input signal.

Using computed tomography, it is possible to view a single plane inside the scanning volume. As the differential slices of the disks pass through this plane, they present the potential for generating time-varying input signals by placing rings of small slots at constant radius. These slots make up one half of an “event pair”, the other half consisting of an equally sized section of plastic. A simple, organized method of

determining the number of event pairs that would be necessary to simulate the desired frequency was needed. Starting with the drive shaft speed, the number, size, and spacing of the event pairs were then determined as functions of the rotational frequency of each planetary gear assembly.

The drive shaft speed was increased in increments of 10 RPM through successive iterations of the analysis. The successive steps of the analysis for a drive shaft speed of 10 RPM are shown in Tables Table 7, Table 8, Table 9, and Table 10. Grayed-out portions of the tables denote results that were physically unobtainable, or not used in the final prototype.

The first step was to calculate the frequency at which the disks themselves rotate, as seen in Table 7. IG refers to the internal gear, and the gear ratio refers to the gear ratio between the specified sun gear and the internal gear of the assembly.

Parameter	Value	Units
Shaft Speed	10	rpm
Gear Ratio-16	0.16	-
IG 1 Speed	1.6	rpm
IG1 Frequency	0.03	Hz
Gear Ratio-34	0.34	-
IG 2 Speed	3.4	rpm
IG2 Frequency	0.06	Hz

It is possible to define a temporal frequency in terms of event-pairs per second. As such, the next step in the analysis was to determine the number of “event-pairs” necessary to generate the desired frequency. An event-pair (EP) denotes a change in the material properties that generates the signal. For instance, as the disk rotates through a plane in space, the event-pairs are created by the disk material and the empty slot space.

The scanner is able to detect or “see” a signal because of these event-pairs. The number of EPs was calculated by dividing the desired input frequency by the frequency of rotation of each disk. Table 8 shows calculations for the number of EPs necessary to simulate the desired frequency on each respective planetary gear assembly. At low frequency, it was not possible to achieve integer values of input frequencies.

Desired Freq. (Hz.)	Number of EPs	
	16 tooth gear stage	34 tooth gear stage
4	150	70.59
2	75.000	35.29
1	37.500	17.65
0.5	18.750	8.82
0.25	9.375	4.41
0.125	4.688	2.21
0.0625	2.344	1.10
0.03125	1.172	0.5515

Table 9 shows the frequency error analysis performed to determine the closest approximation to each input frequency by using integer numbers of event pairs.

Table 9: Frequency error analysis				
Integer EPs		Actual Frequency		Percent Error
N tooth gear stage				
16 tooth	34 Tooth	16 Tooth	34 Tooth	
150.00		4.00		0%
75.00		2.00		0%
38.00		1.01		1%
19.00		0.50667		1%
	4.00		0.227	-10%
	2.00		0.1133	-10%
	1.00		0.0567	-10%

Table 10 shows calculations to determine the required arc length of each cut in an event pair. The total event pair arc length includes that of the cut, and the corresponding section of plastic.

Table 10: EPs calculations		
Circle	360	degrees
10 RPM Shaft Speed		
Number of EPs	EP Size	EP Spacing
150	1.200	1.200
75.00	2.400	2.400
38.00	4.737	4.737
19.00	9.474	9.474
4.00	45.000	45.000
2.00	90.000	90.000
1.00	180.000	180.000
0.50	360.000	360.000

SolidWorks™ was then used to generate solid models of each phantom EP disk using the results of Tables Table 8, Table 9, and Table 10. The EP spacing column seen in Table 10 refers to the distance from the beginning of one arc-shaped cut to the next. The large hole in the middle of each phantom is used to mount each on an internal gear.

Figure 10 shows the location of cuts on the phantom driven by the 34 tooth sun gear. Figure 11 shows the same for the phantom driven by the 16 tooth sun gear. Using two stages with the phantoms placed close together provides a very wide range of frequencies. These two stages could be located near the scanner’s sweet spot. Other sets of two stages could also be located along the drive shaft to allow for a comparison of temporal resolution as a function of position within the scanning bore.

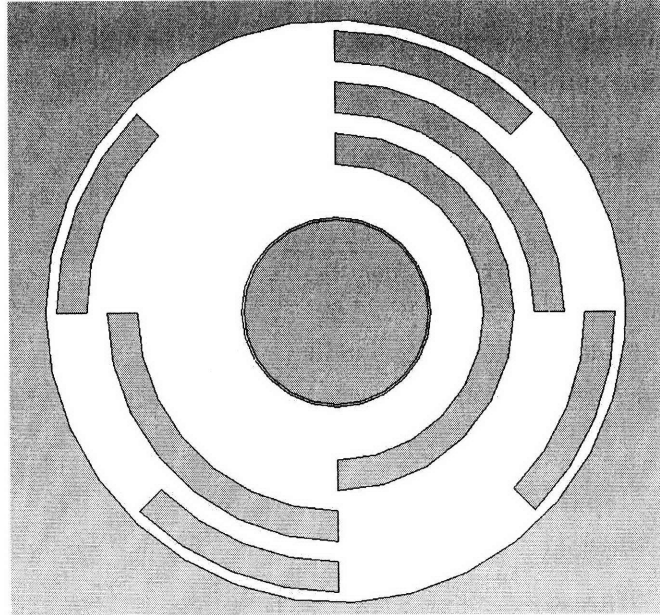


Figure 18: The frequency simulation disk driven by the 34 tooth sun gear.

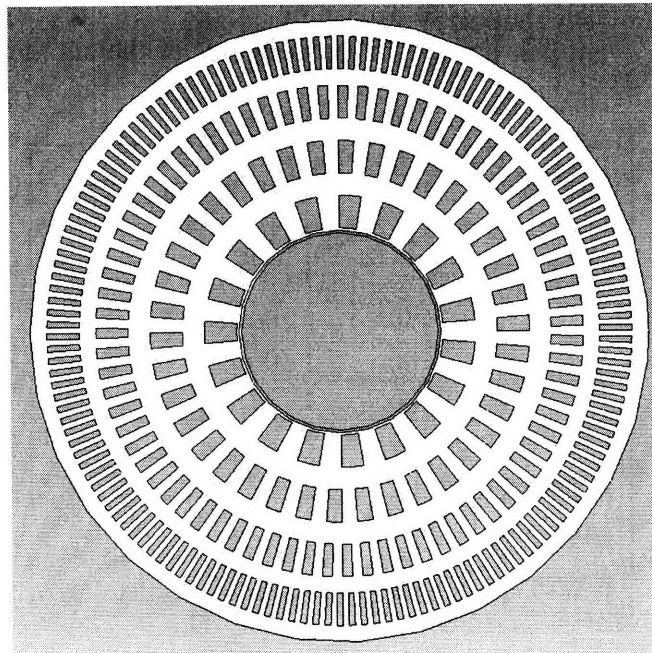


Figure 19: The frequency simulation disk driven by the 16 tooth sun gear.

Drive shaft speed was also examined in order to determine its effect on the most accurately simulated frequencies. Table 11 shows the results of analysis for driveshaft speeds of 20 and 40 RPM. As a result of the increase in speed, the event pair sizes required to simulate slower frequencies increased to unobtainable values. Note that as the drive shaft speed increased, the number of the EPs required in order to simulate small frequencies such as $1/16^{\text{th}}$ Hz, increases while the size of the EPs decreases.

Table 11: Calculation of Event Pair arc length for driveshaft speeds of 20 and 40 RPM.		
20 RPM Shaft Speed		
Number of EPs	EP Size	EP Spacing
75	2.400	2.400
38.00	4.737	4.737
19.00	9.474	9.474
9.00	20.000	20.000
2.00	90.00	90.000
1.00	180.00	180.000
0.50	360.00	360.000
0.25	720.00	720.000
40 RPM Shaft Speed		
Number of EPs	EP Size	EP Spacing
38	4.800	4.800
19.00	9.474	9.474
10.00	18.000	18.000
5.00	36.000	36.000
1.00	180.00	180.000
0.50	360.00	360.000
0.25	720.00	720.000
0.13	1440.00	1440.000

The grayed-out cells in the table above denote an EP configuration where the sum of the arc length of the cut and the required arc spacing between the cuts is larger than 360 degrees.⁶ This makes it impossible to create this specific configuration of event pairs.

The temporal resolution phantom was scanned in a Siemens Medical Solutions Somatom Sensation 64 VCT scanner⁷ at Massachusetts General Hospital in Boston, Massachusetts. Images generated from the scanner showed clearly the effects of the t-MTF throughout all 7 bands simulating frequencies.

Figure 12 shows a cross-sectional image of the TRP, generated using the Siemens Sensation 64. The light-gray and black areas subtended by small gray squares are the event pairs. Note the property of the internal gear assemblies in this image that they are essentially symmetrical across the driveshaft.

⁶ It is impossible to have a cut, at constant radius, with an arc subtending an angle greater than 360 degrees.
⁷ Siemens Medical Solutions (www.siemens.com).

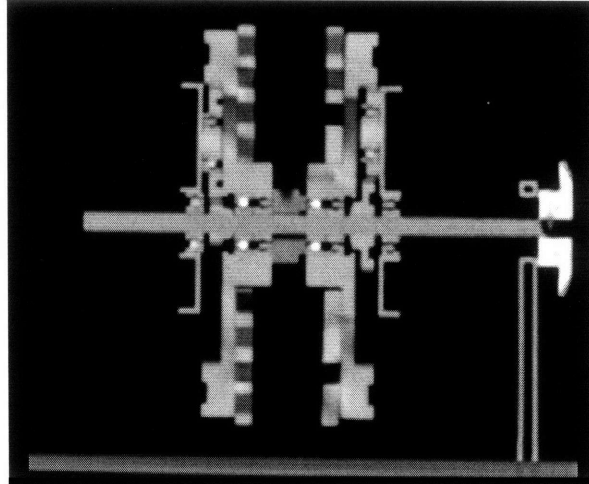


Figure 20: Cross-section image of the Iteration II TRP generated using a clinical scanner.

2.8 Phantom Disk Design - Iteration II (Universal Phantom)

For the third iteration of the TRP, the design of the phantom disks was changed to account for the fact that there were now four planetary gear drives. The optimal phantom design (including the size and spacing of event pairs) had not yet been determined. The size of the smallest event pairs on the first iteration phantom disk made them very expensive to manufacture, and this would create monetary problems when manufacturing new phantom designs. A new phantom design was required that was cheaper and easier to manufacture.

One of the simplest and easiest ways to reduce the cost of a machine is to reduce the overall part count. As such, the event pair analysis utilized to calculate EP size for the first iteration disks was repeated, this time for all of the planetary gear assemblies used in the third iteration TRP. It was postulated that it was possible to achieve a spread of input frequencies of comparable size variation of the input signal frequency simply by varying the gear ratios within each planetary gear drive. Doing this would achieve two things:

1. Reduce part count by requiring only one single phantom disk to be manufactured, instead of four individual phantom disks.
2. Reduce the cost of successive iterations of the TRP. In order to fine-tune the performance of the device, several phantom design iterations could be required in order to determine the optimal phantom design.
3. Prevent incorrect assembly of the TRP by making all of the phantom disks interchangeable with each planetary gear assembly.

The variation in input signal frequency would be achieved simply by varying the planetary gear ratio driving each phantom. Each planetary gear set would drive a phantom identical to that driven by the other planetary gear sets (thus the name “universal phantom”) at a different rotational velocity, generating different input signal frequencies. In the second iteration, this signal frequency spread was achieved by varying both the number of event pairs on each disk as well as the gear ratio of the planetary gear drives.

If it was possible to achieve the same performance with a “universal phantom” the overall cost of the phantom would be reduced.

Table 12 shows the end result of the analytical procedure used to create the second generation phantom disks, utilizing a shaft speed of 10 RPM. The numbers in bold are sun gear tooth counts. If the shaft speed is decreased to approximately 1 RPM, then the same lower bound for the frequency spread can be achieved (on the order of 1/100th Hz) as in the second iteration TRP. Figure 21 shows the first iteration of the universal phantom disk.

Sun gear teeth	16	24	32	34
Gear Ratio	0.16	0.24	0.32	0.34
RPM	1.6	2.4	3.2	3.4
Frequency	0.0267	0.0400	0.0533	0.0567
# EPs				
	Simulated Frequencies			
20	0.5333	0.8000	1.07	1.13333
30	0.8000	1.20	1.60	1.70
50	1.33	2.00	2.67	2.83
75	2.00	3.00	4.00	4.25
100	2.67	4.00	5.33	5.67

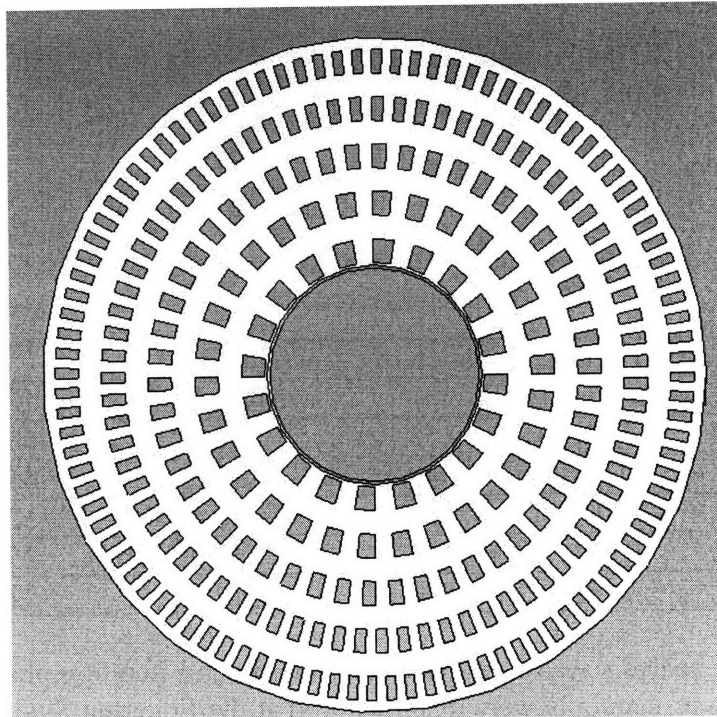


Figure 21: The first iteration universal phantom disk.

2.9 Universal Phantom Iteration II

The width of a scan executed by the scanner when imaging the TRP is 2.4 cm. In order to assure that each scan images a full period of the input signal, the minimum event pair width was thus defined to be 2.4 cm (approximately 0.94 inches). It was necessary to create rings of event pairs that satisfy this design parameter. Table 13 shows the calculation of the required number of event pairs. The column labeled “Diameter (in)” gives the inner diameter of each event pair ring, and is used to calculate the circumference of each event pair ring.

By dividing the circumference by the minimum allowable width of a single event pair (0.94 inches), an approximation of the number of event pairs that can be fit in each ring is obtained. These event pair approximations are then rounded down to the nearest integer. This assures that the width of each event pair is larger than the minimum required width.

Table 13: Calculating required number of event pairs

Ring	Diameter (in)	Circumference	# of EPs	Integer
1	1.9	5.97	6.32	6
2	2.7	8.48	8.98	8
3	3.5	11.00	11.64	11
4	4.3	13.51	14.30	14
5	5.1	16.02	16.96	16

In Table 14, the columns labeled as “EPW” describe the “Event Pair Width”. This is found by dividing the integer number of allowable event pairs in each ring by the circumference of each ring, and is done to assure that the minimum size requirement is fulfilled by each event pair ring. The cut size is found by dividing the number of degrees in a circle (360) by the integer number of event pairs, and the cut spacing is equal to twice the width of a single cut. This assures that the input signal to the tomographic imaging device is a square wave.

Table 14: Determination of event pair size

EPW (new)	EPW (cm)	Cut size (deg.)	Spacing (deg)
1.01	2.55	30.0	60.0
0.94	2.40	22.5	45.0
1.00	2.54	16.4	32.7
1.04	2.63	12.9	25.7
1.00	2.54	11.3	22.5

After this analysis was completed, and the second iteration phantom modeled in SolidWorks™, four phantoms were manufactured at the Edgerton Student Shop at MIT⁸. Figure 22 shows the solid model of the second iteration universal phantom, and Figure 23 shows one of the four phantoms manufactured using rapid prototyping at MIT.

⁸ Thanks to Mark Belanger for setting up and operating the 3-D printer!

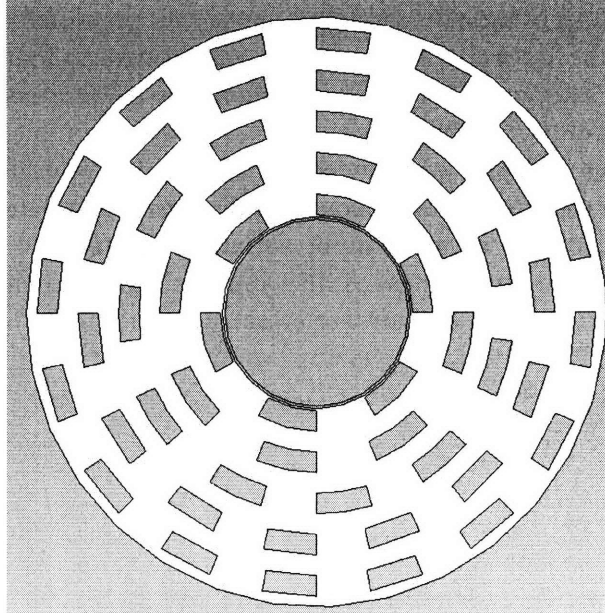


Figure 22: The second iteration universal phantom disk. Notice the increase in the event pair size.

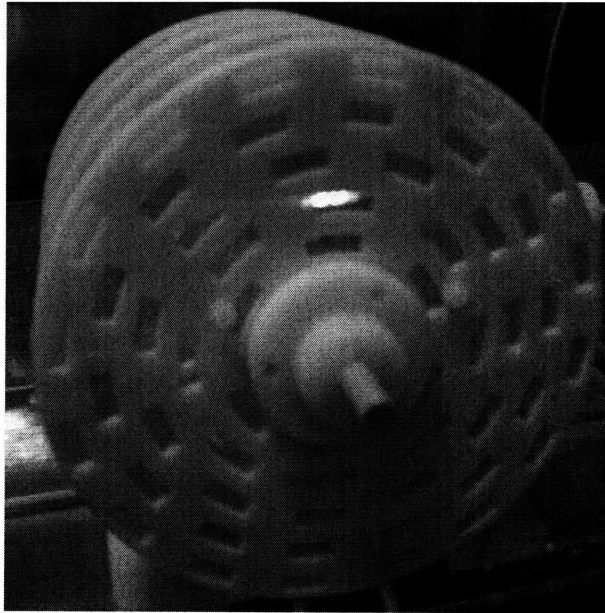


Figure 23: Second iteration universal phantom, 3-D printed at the Edgerton Student Shop at MIT.

3. Results and Discussion

3.1 TRP Iteration II (*Proof-of-Concept*)

Figure 24 shows the raw image data generated using second-iteration prototype. As can be seen in the figure, for low frequencies the sinusoidal variation of the input signal is quite apparent. For high frequencies, there is almost no modulation, represented as an essentially horizontal line. This is the result of the scanner not being able to resolve

the individual crests and troughs in the input signal. As previously stated, an analogy to spatial MTF allows the temporal resolution to be defined as that signal frequency for which there is 10% temporal MTF. The frequencies of these signals are above the temporal resolution of the CT scanner.

Each particular frequency produced by the TRP was registered by the scanner with different fidelity: the lower frequencies preserve the modulation in the input signal, while the higher frequencies blur the input variation completely. In other words, the maximum and the minimum values of the input signal, which ideally should vary between the HU value of plastic and air, are affected by the signal frequency.

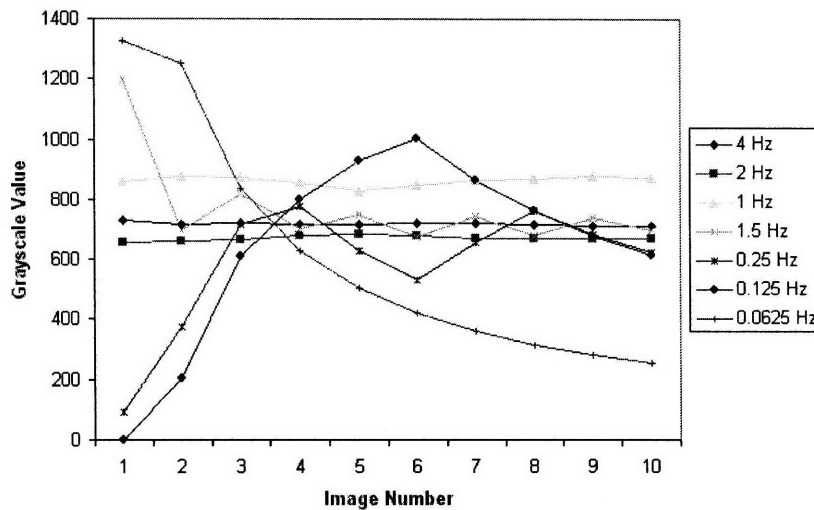


Figure 24: Modulation data. Each frequency produced by the TRP was registered by the Sensation-64 scanner and was assigned a grayscale value (measured in HU).

A Matlab⁹ script was used to plot the t-MTF function from the raw image data. The Modulation vs. Frequency curve (i.e., the t-MTF) is presented in Figure 14 for the Sensation-64. There is an apparent decay of input signal modulation as the signal frequency is increased. Approximately 82% modulation is seen at a frequency of 1/16th Hz, and approximately 1% modulation at 4 Hz. This makes sense intuitively, because as an object moves faster under the scanner, its features become less distinguishable and the grayscale values obtained become more blurred.

⁹The MathWorks Inc (<http://www.mathworks.com/>).

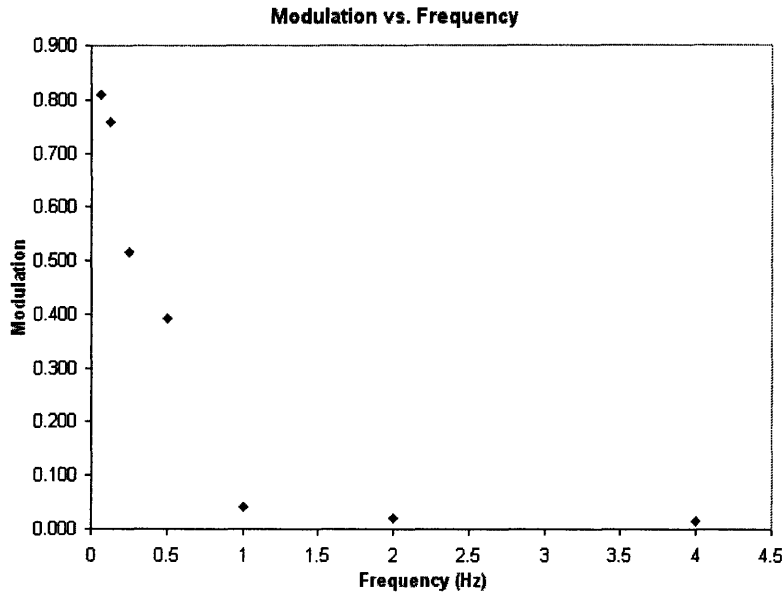


Figure 25: The t-MTF graph for the Sensation 64 scanner. Gantry was operated at a speed of one rotation per second. The temporal resolution, defined as the frequency at which there is 10% modulation transfer, is approximately 0.8 Hz.

After a successful first test with the Sensation 64 scanner, it was determined that the system should be modified so as to be very easily portable. The portability requirement stems from the goal of making this machine available to hospitals and research institutions that use tomographic scanners and that would use this device to analyze several different machines. The rotation rate of the device during initial data acquisition was estimated to be 10 RPM.

3.2 TRP Iteration III

Data collected using the third iteration Temporal Resolution Phantom, with the first iteration of the Universal Phantom, was used to calculate the temporal resolution of two different CT scanners (at this time, the second iteration universal phantom is still being tested). The data collection was performed at Massachusetts General Hospital on a GE Lightspeed 64 and a Siemens Somatom Sensation 64. Each scan, utilizing all 4 phantoms in the third iteration, generated 20 data points (4 disks with each disk containing 5 input frequencies).

There were 4 scans performed using each scanner, resulting in 80 data points collected per scanner overall. Additionally, the design of the phantom created an overlap in the range of data points. For example, the first scan would cover the spread from 0.01 Hz to 0.8 Hz, and the second scan would cover the spread from 0.6 Hz to 1.5 Hz. In this way, continuity of the data is assured, as seen by the smooth curves in the following plots.

In Figure 26 a plot of the temporal MTF for both of the scanners is shown. When this plot is compared to Figure 15, we see an almost identical monotonic decline in temporal modulation transfer. Figure shows a plot used to determine each scanner's temporal resolution. The temporal resolution is the frequency at which there is 10% temporal modulation transfer from the physical space to the image space.

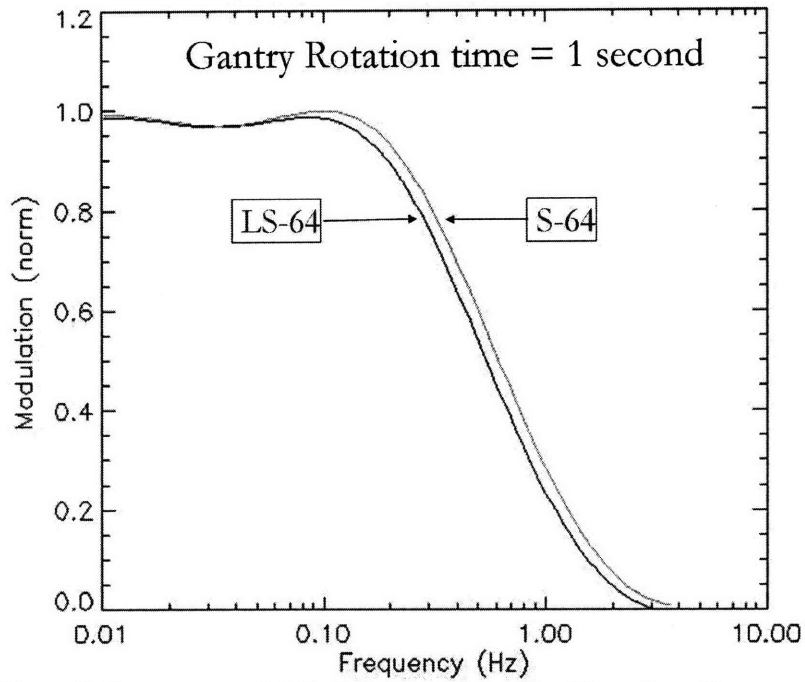


Figure 26: Plot of the temporal Modulation Transfer Function for two different CT scanners.

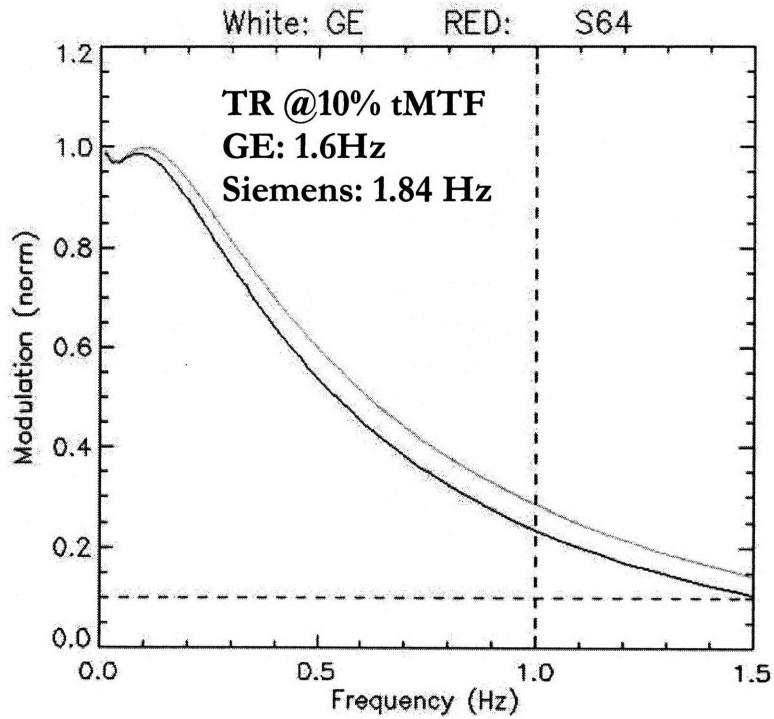


Figure 27: The temporal resolution is the frequency at which each scanner achieves 10% modulation transfer. For the GE, this is 1.6Hz, and for the Siemens, this is 1.84 Hz.

4. Conclusions

The goal of this project is to make available an accurate and repeatable device to be used for determining the temporal resolution of tomographic imaging devices of any model from any vendor. It has been demonstrated that the concept of t-MTF, implemented utilizing the Temporal Resolution Phantom (TRP), meets this goals. It has been shown that the frequency content of the image of an object is directly related to the frequency content of the object itself. The TRP is able to accurately generate input frequencies that are detectable by tomographic scanners in order to characterize a temporal response.

While the first implementation of the TRP was described in the context of a CT scanner, the concept of t-MTF, as well as the calibration phantom described above, is very general. For example, the current TRP design could be easily adapted for an MRI scanner, because it is made entirely of plastic. The only issue that would need to be addressed in order to make this device MRI compatible is the DC motor. It would needs to be moved outside of the influence of the magnetic field generated by the MRI machine. Similar adaptations are also possible to make this device compatible with ultrasound, and other tomographic modalities.

Currently, the device has a patent pending through the MGH Patents and Licensing Office. The design of a third iteration, which will have a similar volume enclosure as present in designs of static imaging phantoms, is currently being finalized.

References

- [1] Kane, S. A., 2003, *Introduction to Physics in Modern Medicine*, Taylor and Francis, New York, pp. 147-166, pp.189-197.
- [2] Gupta, R., Grasruck, M., Suess, C. et al. “Ultra-high resolution flat-panel volume CT: fundamental principles, design architecture, and system characterization.” *Eur. Radiol.* 2006 Jun; 16(6): 1191-205. Epub 2006 Mar 10
- [3] Boreman, G. D., 2001, *Modulation Transfer Function in Optical and Electro-Optical Systems*, SPIE, Washington, pp. 7-17, pp. 35-44, p. 59.
- [4] Lang, S. Y. T., 2004, “Graph-theoretic modeling of epicyclic gear systems”, Elsevier, *Mech. Mach. Th.* **40** (511-529), pp. 513-521.
- [5] Slocum, A. H., 2007, *FUNdaMENTALS of Design*, Topic 6 – Power Transmission Elements II, <http://pergatory.mit.edu/2.007>.
- [6] Graham, M., Slocum, A., Moreno Sanchez, R., “Teaching high school students and college freshman product development by Deterministic Design with PREP”, *ASME Journal of Mechanical Design* (Special Issue on Design Engineering Education), July 2007, Vol. 129, pp 677-681.
- [7] Slocum, A. H., 2007, *FUNdaMENTALS of Design*, Topic 3 – *FUNdaMENTAL* Principles, <http://pergatory.mit.edu/2.007>.